Subsurface contrast due to friction in heterodyne force microscopy

Verbiest, G.J.; Oosterkamp, T.H.; Rost, M.J.

Subsurface contrast due to friction in heterodyne force microscopy

OPEN ACCESS
IOP Publishing
Nanotechnology

Nanotechnology **28** (2017) 085704 (8pp)
doi:10.1088/1361-6528/aa53f2

Subsurface contrast due to friction in heterodyne force microscopy

G J Verbiest[1], **T H Oosterkamp and M J Rost**[2]

Huygens-Kamerlingh Onnes Laboratory, Leiden University, Niels Bohrweg 2, 2333 CA Leiden, The Netherlands

E-mail: Verbiest@physik.rwth-aachen.de and Rost@physics.leidenuniv.nl

Received 26 September 2016, revised 12 December 2016
Accepted for publication 15 December 2016
Published 18 January 2017

Abstract

The nondestructive imaging of subsurface structures on the nanometer scale has been a long-standing desire in both science and industry. A few impressive images were published so far that demonstrate the general feasibility by combining ultrasound with an atomic force microscope. From different excitation schemes, heterodyne force microscopy seems to be the most promising candidate delivering the highest contrast and resolution. However, the physical contrast mechanism is unknown, thereby preventing any quantitative analysis of samples. Here we show that friction at material boundaries within the sample is responsible for the contrast formation. This result is obtained by performing a full quantitative analysis, in which we compare our experimentally observed contrasts with simulations and calculations. Surprisingly, we can rule out all other generally believed responsible mechanisms, like Rayleigh scattering, sample (visco) elasticity, damping of the ultrasonic tip motion, and ultrasound attenuation. Our analytical description paves the way for quantitative subsurface-AFM imaging.

S Online supplementary data available from stacks.iop.org/nano/28/085704/mmedia

Keywords: heterodyne force microscopy, contrast mechanism, subsurface, friction, ultrasound, atomic force microscopy, excitation scheme

(Some figures may appear in colour only in the online journal)

1. Introduction

Many fields of research are in need of a nondestructive way of imaging nanometer-sized subsurface features. To this end, ultrasound was combined with atomic force microscopy (AFM) to invent ultrasound force microscopy (UFM) in 1993 [1] and Waveguide-UFM in 1996 [2]. The combination of these two techniques led to the development of heterodyne force microscopy (HFM) in 2000 [3, 4]. HFM makes use of two ultrasound waves at slightly different frequencies, one of which is sent through the sample and the other through the cantilever. The mixed, heterodyne signal (amplitude and phase) at their frequency difference contains possible subsurface information at an experimentally accessible frequency [5]. Regarding subsurface imaging, HFM is considered to be the technique that delivers the highest sensitivity, the best resolution, and the least damage to the sample/surface: the smaller the amplitudes are of the ultrasonic vibrations, the higher is the contrast [6]. Therefore, HFM measurements penetrate the sample at most a few nanometer, while comparable UFM measurements typically need ultrasonic amplitudes that are large enough to generate a tip induced stress field that extends down to the depth of the buried structures. This is because UFM relies on *feeling* through the sample [1, 7, 8], while HFM picks up the soundwave that traveled through the sample, like a radio [9]. Note that there exists a unique report, in which UFM is applied even at GHz

[1] Current address: JARA-FIT and 2nd Institute of Physics, RWTH Aachen University, D-52074 Aachen, Germany.
[2] Author to whom any correspondence should be addressed.

frequencies: the observed contrast relies on diffraction [10]. Using HFM, we will show here that it is possible to observe 20 nm large Au nanoparticles below 82 nm of polymer, although we use an (combined) ultrasonic vibration amplitude of only 1.71 nm and indent at maximum 6 nm into the sample.

Using HFM, subsurface images with remarkable contrast and resolution have been reported [3, 11–22], like the detection of 17.5 nm large gold nanoparticles buried at a depth of 500 nm in a polymer [14]. Surprisingly, the generated contrast clearly exceeds the background variations in these images, although the size of the nanoparticles is only a fraction of the sample thickness, and the lateral fingerprint *on* the surface (resolution) is equal to the diameter of the nanoparticles. Both observations are hard to understand, if one considers the wavelengths of the ultrasonic excitations, which is in the order of mm's and therefore much larger than both the size of the nanoparticles (nm's) and their depth below the surface (up to μm's). Unfortunately, none of the published HFM experiments provides quantitative information on the measured amplitude and phase range, on the applied contact force during the measurement, and on the precise excitation scheme in combination with the resonance frequencies of the cantilever.

To pave the way for quantitative subsurface measurements, it is of crucial importance to understand the physical contrast formation mechanism [23]. This requires a detailed, quantitative understanding of the ultrasound propagation within the sample [24], the cantilever dynamics [6, 7, 25–27], nonlinear mixing [9, 28, 29], the explicit excitation scheme, the resonance frequency spectrum of the cantilever [2, 30, 31], resonance frequency shifting [31], and the response to variations in the tip–sample interaction [31–34] that are determined by the local elasticity and adhesion of the sample. All these factors can significantly change the heterodyne signal leading to a measurable contrast. Published HFM experiments that provide (at least some) quantitative information are scarce [15] and the actual depth of the subsurface features is confirmed independently only in [13].

In this paper, we present a full quantitative analysis that addresses all physical contrast mechanisms we can imagine to explain our experimental observations on a well characterized sample. This quantitative analysis is the first of its kind and has become only possible, due to series of our earlier work, in which we focused on the generation of the signal at the difference frequency in HFM: first we showed that the ultrasound amplitude of the cantilever does not decrease when indenting into the sample [6, 25], which means the cantilever works only as a pickup. Based on this, we derived full analytical equations that describe the generation of the heterodyne signal at the difference frequency, which we confirmed both experimentally and via simulations [9, 25]. To derive hard numbers from our model, one only needs to know the applied ultrasound waves, which are set by the user, and the tip–sample interaction, which can be measured experimentally. Note that the exact (theoretical) tip–sample model is not important as long as it quantitatively matches the experimentally measured interaction [9]. Equipped with this insight, we show that Rayleigh scattering [24] would produce a contrast that is orders of magnitude smaller than in the experiment. By calculating the cantilever dynamics for different tip–sample interactions, we show that variations in sample elasticity indeed can lead to contrasts that are, in magnitude, comparable to the experiments. However, we can also rule out this mechanism, as the contrast is inverted with respect to the experimentally observed one. The only remaining possibility is dissipation! As we can also exclude tip damping and ultrasound attenuation, we finally conclude that *friction* at *shaking* nanoparticles is the responsible physical contrast mechanism. Additional evidence for this comes from an estimate of the involved energy dissipation.

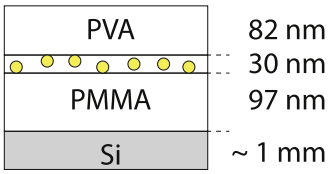

Figure 1. Schematic cross section of the final sample stack: on the silicon wafer, we have (from bottom to top), a 97 nm PMMA layer, a 30 nm PVA layer that also contains gold nanoparticles with a diameter of 20 nm, and a 82 nm PVA layer (see methods and supplementary notes 1 and 2 for more details).

Our analysis shows that the contrast strongly depends on the applied contact force and the precise ultrasonic excitation scheme with respect to the resonance frequencies (and their shifts) of the cantilever.

2. Methods

All measurements described in this paper are performed with a Digital Instruments (Nanoscope 3) AFM that we equipped with a homebuilt cantilever holder as well as ultrasonic sample transducer [4].

As a quantitative analysis of the contrast mechanism is impossible without a well-characterized sample, we carefully prepared a stack consisting of the following layers (from bottom to top, see figure 1): a Si wafer with native oxide, a ~97 nm thick PMMA layer, a 30 nm thick PVA layer with embedded gold nanoparticles (diameter 20 nm), and a 82 nm thick PVA top layer. The density of the gold nanoparticles was determined via AFM and SEM to be 0.7 ± 0.6 particles μm^{-2}. The precise sample preparation as well as its detailed characterization, in which we even determined the depth of the Au nanoparticles with an independent measurement based on Rutherford backscattering, is described in detail in supplementary note 1 and 2.

In our HFM experiment, we chose the ultrasonic excitation frequencies of both the tip and the sample as well as the difference frequency *off* resonance, i.e. not on (or within the width) of a resonance peak of the cantilever, see figure 2. We call this excitation scheme *off–off resonance*. The first *on/off* indication describes whether f_{diff} (heterodyne signal) is tuned to a resonance frequency of the cantilever, whereas the second *on/off* indication describes whether f_t (ultrasonic tip excitation) is tuned to a resonance. This leads to four different excitation schemes, of which we evaluate also the *off–on* scheme in more detail in supplementary note 8.

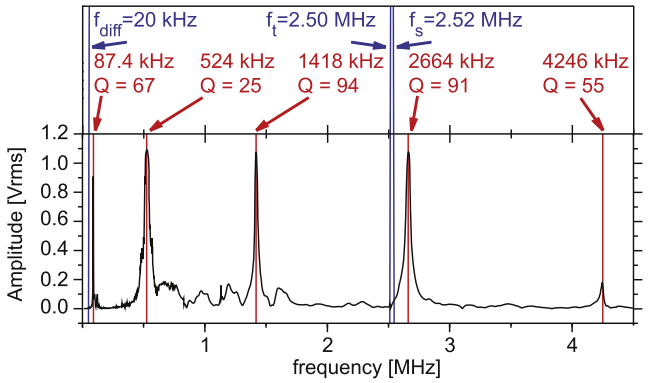

Figure 2. Experimental excitation scheme: this scheme falls into the class of *off–off resonance* excitation, see methods. The vibration spectrum of the free hanging cantilever is also shown. A red line indicates a resonance frequency: its value and corresponding Q-factor are indicated in the top panel. The blue lines indicate the applied excitation frequencies of the tip $f_t = 2.50$ MHz, the sample $f_s = 2.52$ MHz, and the difference frequency $f_{diff} = 20$ kHz, which all do not coincide with a resonance frequency of the cantilever.

3. Results

To enable a quantitative analysis of our measurements, we carefully prepared a sample with 20 nm large gold nanoparticles embedded 82 nm below the surface, see figure 1. The preparation as well as the independently determined characterization of the sample with AFM, Rutherford backscattering spectroscopy (RBS), and scanning electron microscopy (SEM) is described in supplementary notes 1 and 2.

As the explicit excitation scheme is of crucial importance for the measured HFM contrast, figure 2 shows our particular experimental choice, called *experimental scheme*, with an *off–off resonance* excitation scheme (see methods for the definition of schemes).

We calibrated the spring constant to be 2.7 N m^{-1} using the thermal noise method [35]. Then, we determined the spring constants of the higher modes by matching the observed resonance frequencies to the ones found in the numerical calculation [31]. By extracting the slope of the analytical mode shape at the free end of the cantilever and comparing it to the one of the fundamental mode, we quantified the vibration amplitude of the cantilever at the ultrasonic excitation frequency to be $A_t = 1.34$ nm. Finally, we used the measured tip–sample interaction together with the simultaneously measured amplitude at the difference frequency A_{diff} to determine the ultrasonic vibration amplitude of the sample: $A_s = 0.37$ nm. This method is described in detail in [9, 25].

Figure 3 shows the actual HFM experiment with simultaneously measured height (a)–(d), amplitude A_{diff} (e)–(h) and phase ϕ_{diff} (i)–(l) of the difference frequency f_{diff} for various contact forces F_c. Feedback was performed in contact mode operation. The contact force F_c is decreased from top to bottom: 163, 115, 67, and 2.4 nN. The gold nanoparticles are visible in the height, A_{diff}, and the phase at $F_c = 163$ nN. The observed density of 1.2 particles μm^{-2} fits the independently determined density (see supplementary note 1). Most of the gold nanoparticles are still visible at $F_c = 115$ nN, although

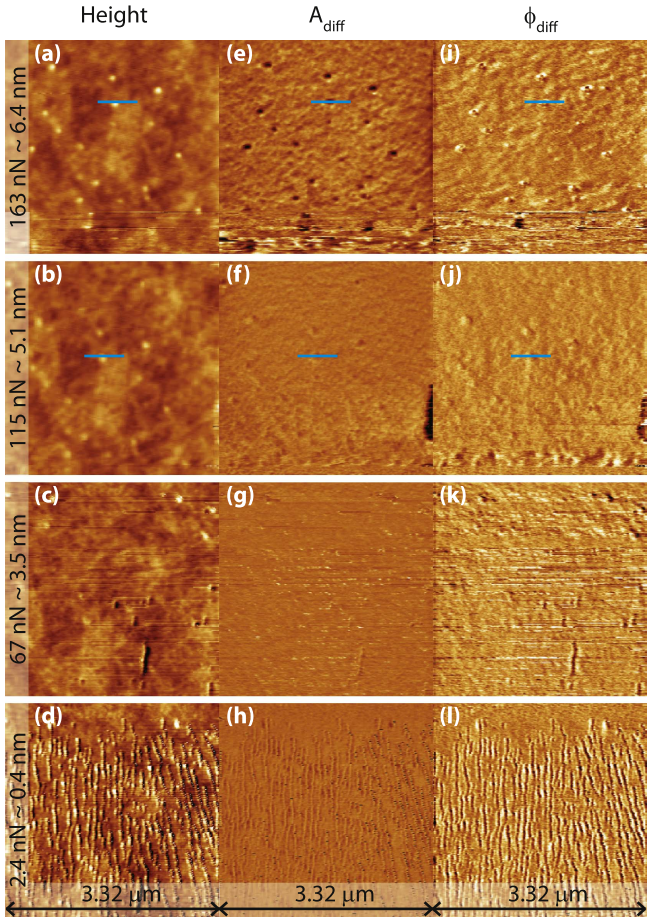

Figure 3. HFM measurements for different contact forces: from left to right measured simultaneously: the height (a)–(d) and both the amplitude A_{diff} (e)–(h) and the phase ϕ_{diff} (i)–(l) of the difference frequency. The contact force F_c as well as the resulting *average indentation* into the sample are indicated at the left in the height images. The gold nanoparticles are only visible at a contact force of 163 and 115 nN. At these forces, they are not only visible in A_{diff} and ϕ_{diff}, but also in the height image. We 'loose' the nanoparticles in the height, A_{diff}, and ϕ_{diff} with decreasing force. At a $F_c = 2.4$ nN, we observe that we damaged the surface, while measuring at higher forces. All height, A_{diff}, or ϕ_{diff} images have the same (color) range such that the contrast for different contact forces can be compared directly. We provide typical cross sections with absolute values of the height, A_{diff}, and ϕ_{diff} at the positions of the nanoparticles in figure 4.

the contrasts are significantly reduced. At lower forces, we do not (or just barely) detect any nanoparticles, which supports the RBS measurements that the gold nanoparticles are indeed fully buried under a 82 nm thick PVA layer. Considering the tip indentation depths of less than 6.5 nm (note that this is different from the total height variation, see left side in figure 3) in combination with the total ultrasonic vibration amplitude of the sample and the tip of $A_s + A_t = 1.71$ nm, it is striking that we see the nanoparticles in the height images: the total ultrasonic vibration amplitude is at least ten times smaller than the depth of the nanoparticles[3] (82 nm). In

[3] We only see the nanoparticles also in the height, if we have both ultrasound signal switched on. This surprising effect is subject to an own publication that we are currently preparing.

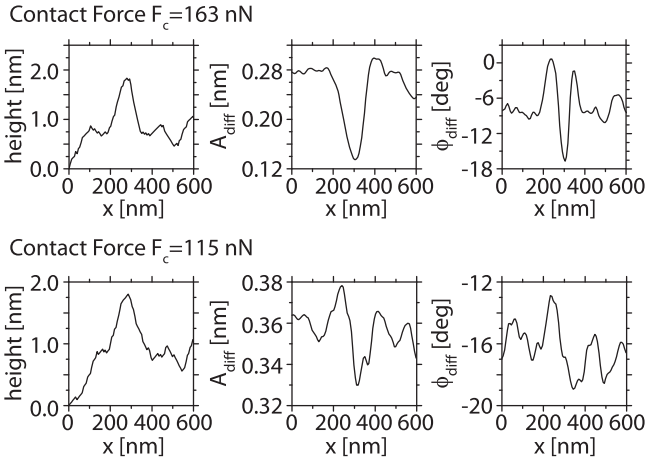

Figure 4. Cross sectional lines of the height, A_{diff} and ϕ_{diff} at the position of the blue lines in figure 3: the top panels are for a contact force of 163 nN, whereas the bottom ones are for 115 nN. For a given contact force, the blue lines in figure 3 are exact on the same location. As the height, A_{diff}, and ϕ_{diff} are recorded simultaneously, the same pixel in the different cross sectional lines is taken at exactly the same time. At a contact force of 163 nN, the height, A_{diff}, and ϕ_{diff} clearly show strong contrasts, whereas at 115 nN the contrasts in A_{diff} and ϕ_{diff} are almost of the same size as the corresponding background variations.

comparison, subsurface contrast in UFM or waveguide-UFM is only obtained, if the tip induced stress field generated by the sound wave extends all the way down to the depth of the subsurface features. In [8] they need an ultrasonic amplitude of 27 nm to see the buried particles at a depth of 34 nm, while our amplitude is only 1.71 nm and we still see the particles even at a depth of 82 nm.

At $F_{\mathrm{c}} = 2.4$ nN, we probe the attractive part of the tip–sample interaction as the total ultrasonic vibration amplitude is smaller than the indentation depth and recognize that we have damaged the surface slightly, while measuring earlier at higher contact forces. The root-mean-square amplitude of the induced height variation is only 0.9 nm. Please note that in UFM the sample is significantly more damaged, due to the required large ultrasound amplitudes.

At $F_{\mathrm{c}} = 2.4$ nN, both the A_{diff} and the ϕ_{diff} image show a clear correlation with the height. As the cantilever mainly probes the attractive part of the tip–sample interaction during an oscillation, the effective contact area of the tip depends on the height variations of the sample: it is much smaller on a mountain than in a valley. Adhesion is directly proportional to the contact area and a variation of it indeed leads to a variation in both the amplitude and the phase of the subsurface signal [9]. We conclude that variations in the adhesion do generate a contrast in A_{diff} and ϕ_{diff}.

To quantify the contrasts of the gold nanoparticles in figure 3, we extract from cross sectional lines, as shown in figure 4, the average values above the nanoparticles for the height, A_{diff}, and ϕ_{diff} with respect to their background, see table 1.

Let us first compare the experimental values with the expected contrast based on Rayleigh scattering [24], for which we have to normalize the amplitudes A_{diff} with respect to their background amplitudes A_{b}. At $F_{\mathrm{c}} = 163$ nN, we measure a normalized amplitude contrast, A_{c}, of -0.44 and a phase ϕ_{diff} of 7.2°. At $F_{\mathrm{c}} = 115$ nN, the normalized amplitude contrast is -0.11 and the phase contrast is 2.9°. Based on Rayleigh scattering, the expected normalized amplitude contrast is 10^{-6} and the phase contrast is 0.1 millidegree for a gold particle with a diameter of 20 nm buried 50 nm deep under a polymer (PMMA) [24]. As the experimentally observed normalized amplitude contrast is 5 orders of magnitude larger (and the phase contrast 4 orders of magnitude) than the theoretically predicted ones, we have to conclude that Rayleigh scattering takes place, but does *not* form a major contribution to the physical contrast mechanism (at least not at MHz frequencies).

Recently, it was elucidated how the heterodyne signal is generated: its magnitude strongly depends on both the applied contact force and the specific characteristics of the tip–sample interaction [6, 9, 25]. In supplementary notes 3 and 4 we show, both experimentally and analytically, that the heterodyne signal depends on the elastic properties of the sample, which is characterized by its Young's modulus E. For sufficiently soft samples, the amplitude A_{diff} *increases* linearly with *increasing* E (see equation (9) in supplementary note 4). Let us, in the following, consider elasticity variations in the sample, due to the presence of the nanoparticles, as a possible contrast mechanism.

From an analytical 1D model, we estimate that the Young's modulus above a gold nanoparticle is ∼10% higher than the Young's modulus of PMMA or PVA, which is 2.4 GPa, see supplementary note 6. Note that we experimentally verified that the Young's modulus of our final sample (stack) indeed equals the Young's modulus of PMMA, see supplementary note 5. To determine the contrast formation based on these elasticity variations, we numerically calculated the motion of the cantilever for different tip–sample interactions using the method outlined in [6]. The result is shown in figure 5, in which we, for reasons of clarity, only show the approach curves. To receive an upper bound on the contrast and to elucidate the contrast formation effect on the basis of small elasticity variations, we consider Young's moduli between 2 and 6 GPa. As the specific vibration spectrum of the cantilever has great influence on the results, we first matched the spectrum used in the calculations to that of our experiment, see supplementary note 7. We call the particular *off–off resonance* excitation scheme that we used in this experiment (see figure 2), *experimental excitation*. The graphical result, see figure 5, shows the corresponding tip–sample interactions and, as a function of the applied contact force, the indentations as well as the amplitudes A_{diff} and phases ϕ_{diff} of the heterodyne signal at the difference frequency. The contrasts at a certain contact force can now be evaluated from the difference in the signals stemming from different elasticities (colors in the graphs). The indentation contrast decreases with decreasing contact force. The amplitude contrast stays almost constant over a large range (and even increases slightly), before it collapses, like the phase contrast, to zero at very small contact forces. The extracted height, amplitude and phase values are listed in table 1. In

Table 1. Comparison between experimentally determined and analytically predicted values: the obtained contrasts in the height, the amplitude A_{diff}, the normalized amplitude A_{c} (for which we also provide the background amplitude A_{b}), and the phase ϕ_{diff} for a contact force of 163 and 115 nN. The contrasts are obtained from different numerical calculations taking into account specific excitation schemes, see supplementary note 8. To receive clear upper estimates, we determined (most of) the contrasts from the differences in the curves of figure 5 between a sample with 2 and 6 GPa. For completeness, we provide, for the *experimental* scheme, also the contrasts obtained from the difference in samples with 2.4 GPa (PVA) and 2.6 GPa (effective elasticity above the nanoparticles, as derived in supplementary note 6).

Method	F_{contact} (nN)	Height (nm)	ΔA_{diff} (pm)	A_{b} (pm)	$A_{\mathrm{c}} = \Delta A_{\mathrm{diff}}/A_{\mathrm{b}}$	$\Delta\phi_{\mathrm{diff}}$ (°)
Experiment	163	2.8	−120	270	−0.44	7.2
	115	1.2	−40	360	−0.11	2.9
Exp. scheme	163	0.08	0.87	17	0.05	0.027
(2.4 → 2.6 GPa)	115	0.03	1.1	21	0.05	0.008
Exp. scheme	163	1.8	17	15	1.1	0.120
(2 → 6 GPa)	115	1.2	32	19	1.7	0.083
Off–off resonance[a]	163	1.8	42	20	2.1	0.014
(2 → 6 GPa)	115	1.3	63	24	2.6	−0.002
Off–on resonance	163	1.8	−0.86	7.0	−0.12	11
(2 → 6 GPa)	115	1.2	−0.23	9.6	−0.02	12

[a] The ultrasound signals are midway between two resonance frequencies.

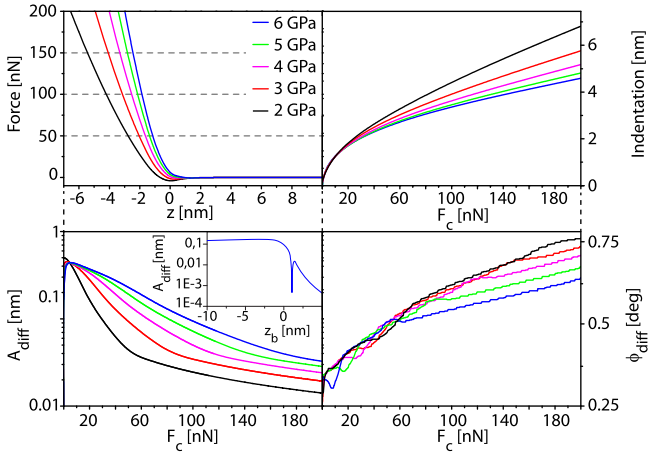

Figure 5. Results for the experimental excitation scheme: we calculated the tip–sample interaction and, as a function of the applied contact force, the corresponding sample indentation as well as the amplitude A_{diff} and phase ϕ_{diff} of the heterodyne signal for different sample elasticities: 2 GPa (black), 3 GPa (red), 4 GPa (magenta), 5 GPa (green), and 6 GPa (blue). The inset in the lower left panel shows A_{diff} for 6 GPa plotted as a function of the height of the cantilever's base, z_{b}, such that a comparison becomes possible with other calculations [6, 9, 25].

addition, to elucidate the effect of different ultrasonic excitation schemes, we also considered an *off–off resonance* excitation, in which both ultrasound signals are midway between two resonance frequencies, as well as an *off–on resonance* excitation, see supplementary note 8. These results are, in addition, tabulated in table 1 for comparison.

The *experimental* scheme with 2.4 GPa (PVA) to 2.6 GPa (effective elasticity above the nanoparticles, see supplementary note 6) perfectly reflects both the sample and the measurement conditions. To receive clear upper bounds, we determined further all excitations schemes from the differences between a sample with 2 and 6 GPa. Starting with the height contrast, we find comparable values between the experiment and the calculated excitation schemes, except for the *experimental scheme* 2.4 → 2.6 GPa. The decrease in height contrast for smaller contact forces F_{c} is reproduced for all cases. Considering the amplitude contrast ΔA_{diff}, the absolute values in the experiment are up to 10 times larger than the calculated ones. Although this already indicates a problem, the most striking issue is the sign of the contrast, which is inverted in comparison with the experiment!

As the (visco)elasticity above the nanoparticle is for sure *increased*, which theoretically leads to a *higher* amplitude A_{diff} (see figure 5 and supplementary note 4), one expects a *positive* amplitude contrast ΔA_{diff} and thus islands instead of holes. In conclusion, although taking place, elasticity variations cannot explain the observed contrast, as it is inverted. Consequently, a different physical mechanism must be present.

Please note that the amplitude contrast inversion of ΔA_{diff} in the *off–on resonance* case is due to its particular excitation scheme with the frequency shift of the 4th mode [31]. Above the nanoparticle, the amplitude reduction of the ultrasonic tip vibration A_{t} is significantly larger than the reduction on the PVA without nanoparticles (see supplementary note 8). This indicates the importance of the precise excitation scheme and the spectrum of the cantilever for each published HFM measurement. Without these information it is impossible to compare measurements or understand them quantitatively.

For the sake of completeness, we shortly turn our attention to the phase behavior. The magnitude of the experimentally observed phase contrast $\Delta\phi_{\mathrm{diff}}$ is only comparable to the special case of the *off–on resonance* excitation scheme. The large phase shift in this scheme is due to the frequency shift of

the 4th resonance: the particular *off–on resonance* excitation scheme makes the tip vibration especially sensitive to phase changes based on frequency shifts [31]. Although much smaller in magnitude, a similar argument holds also for the phase shifts in the *off–off resonance* and *experimental excitation* schemes. Since the ultrasonic tip excitation in the *experimental* scheme is closer to the 4th resonance frequency of the cantilever, we observe a larger phase contrast than in the *off–off resonance* scheme where the excitation of the tip is midway between resonance frequencies.

Summarizing this part, we conclude that the contrast from (small) variations in the sample elasticity results in a much larger contrast than Rayleigh scattering: the order of magnitude is comparable to the experiments. However, variations in sample elasticity *cannot* be the physical contrast mechanism in our HFM experiment, as it would imply an *opposite* sign.

4. Discussion

Ruling out both variations in the tip–sample interaction (elasticity and adhesion) and Rayleigh scattering, the remaining physical contrast mechanism must lead to a significant reduction of the tip amplitude A_t or the sample amplitude A_s above the nanoparticles, as

$$A_{\text{diff}} \sim A_t A_s \Big/ \sqrt{A_t^2 + A_s^2} \qquad (1)$$

(see [9] for the derivation). These reductions can be described as tip or sample damping. Tip damping can also be excluded, as it has been surprisingly shown that A_t keeps 99.7% of its amplitude at a contact force of 25 nN even on a hard sample like Si [25]. Please note that the damping of the resonance frequencies of a cantilever that is in contact with a sample, is generally assumed to be directly proportional to the Young's modulus of the sample [36]. Without significant tip damping, the contrast must be due to a reduction in the sample amplitude. Since a reduction of A_s is expected to occur also on the polymer without nanoparticles, and since A_{diff} is larger above the nanoparticle due to the increase in the effective Young's modulus, we need a mechanism that leads to a strong decrease of A_s *only* above the nanoparticle to overcompensate the increase in A_{diff} such that it effectively leads to a contrast inversion (holes in A_{diff}, see figure 3).

Let us start with a possible vertical motion of the nanoparticles in the polymer matrix. At low ultrasonic sample frequencies, this motion is surely in phase with the excitation. However, if the ultrasonic excitation is above the resonance frequency of the system 'nanoparticle in polymer', the motion will be out of phase leading to a significant reduction of A_s only above the nanoparticles. The problem is, however, that the sample excitation is at 2.5 MHz and that we estimate the resonance frequency of the 'nanoparticle in polymer' system, i.e. the resonance frequency of a mass (the nanoparticle) that is firmly hold by two springs (the PVA layer above and the PMMA layer below), to be ~2.2 GHz (see supplementary note 9). The nanoparticles should, therefore, simply follow the ultrasonic displacements of the polymer.

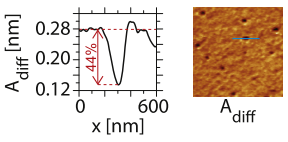

	sign	A_c	ΔA_{diff} [pm]	E_D [eV/osc.]
Measured	**–**	**-0.44**	**-120**	**+2.07**
Rayleigh scattering	–	-10^{-6}	-3.6×10^{-4}	$+5\times10^{-6}$
Tip-sample interaction (incl. excitation scheme)	+	+0.05	+18	-0.27
Tip damping		negligible		
Nanoparticle resonance		not applicable		
Temperature effects		negligible		
Ultrasound attenuation	+	+0.31	+71	-0.45
Total required dissipation	**–**			**+2.79**

Figure 6. Experimentally determined dissipation based on friction at the nanoparticle–polymer interface: we measure holes in A_{diff} that require a dissipation of 2.07 eV osc.$^{-1}$. To provide an overview, we list also the contribution of all other contrast mechanisms that (partly) take place simultaneously. The measured dissipation must be slightly higher than determined (2.79 eV osc.$^{-1}$ instead of 2.07 eV osc.$^{-1}$), as both tip–sample interaction and ultrasound attenuation are not negligible and have, in addition, an inverted sign in the contrast.

Another mechanism worth considering is sample damping (reduction of A_s in equation (1)) by energy dissipation at the nanoparticles. Next to contrast formation based on attenuation or friction, a temperature effect might additionally enhance the contrast, especially if the elasticity of the polymer would have a strong temperature dependence. Therefore, we measure the energy dissipation from our experiment. We determine the sample amplitude A_s (far away from the nanoparticle) in analogy to the method described in [6] . At $F_c = 163$ nN we determine A_s to be $A_s \sim 0.22$ nm. From the A_{diff}-line above the nanoparticle, see figure 6, we determine the reduction of A_{diff} to be 44%. Applying equation (1), A_s must be, therefore, decreased with 41%. A similar determination can be performed for the measurement at $F_c = 115$ nm and one receives that A_s must be decreased with 12%, see figure 4. These measured values can be converted into more appropriate units: using the effective spring constant $k_{\text{eff}} = 4$ N m^{-1} of the sample computed via $(k_{\text{PMMA}}^{-1} + k_{\text{PVA}}^{-1})^{-1}$ (see values in supplementary note 9), the difference in potential energy per oscillation cycle is given by $0.5\, k_{\text{eff}} A_s^2$. Multiplying this value with $2\pi f_s$ results finally in the power dissipation per oscillation cycle. From our measurements we determine 0.53 and 0.86 pW for a contact force of 163 nN and 115 nN, respectively. Following surface science units, this converts to an energy dissipation at the nanoparticles of 2.07 eV oscillation^{-1} of the ultrasonic sample excitation at $f_s = 2.52$ MHz. This dissipation is extremely small, which becomes clear, if one compares it to the cohesive/binding energy of a single Au atom of $E_c = -3.8$ eV. The table in figure 6 provides an overview, in which we list also the contribution of all other contrast mechanisms that (partly) take place simultaneously. The measured dissipation must be slightly higher than determined (2.79 eV oscillation^{-1} instead of 2.07 eV oscillation^{-1}), as the magnitude of both the tip–sample interaction and the ultrasound attenuation are not negligible and have, in addition, an inverted sign in the contrast.

The measured energy dissipation is so small that we can rule out also any temperature effects. The only remaining physical mechanisms that might cause this energy dissipation is ultrasound attenuation *within* the nanoparticles as well as dissipation at the interface *between* the nanoparticles and the polymer.

The ultrasound attenuation for gold is ∼150 times *smaller* than the attenuation for PVA. Therefore the total energy dissipation is *less* at the positions measured above the nanoparticles than at the positions far away from them. This effect results, in comparison to the experiment, again in a wrong sign of the contrast, as A_s should be larger above the nanoparticles. We estimate this resulting energy 'gain' based on a smaller ultrasound attenuation at the nanoparticles to be 0.45 eV oscillation^{-1}. The dissipation that causes the observed contrast, must be increased with this value to overcompensate it and lead to contrast inversion.

In short, we concluded that Rayleigh scattering [24] forms an insignificant contribution to the observed contrast[4]. Elasticity variations within the sample, generate a contrast with opposite sign. As it was shown before that the ultrasound amplitude of the tip remains constant [6, 25], the ultrasonic vibration amplitude of the sample on the surface above the nanoparticle has to be decreased to explain the experimentally observed contrast with holes in A_{diff}. Consequently, ultrasound energy has to be dissipated in or around the nanoparticle. As the ultrasound attenuation in gold is much smaller than in PMMA and PVA, this dissipation *must* happen at the interface between the gold and the polymer. Please note that whatever the exact physical mechanism of this energy dissipation is, one should always label it as *friction* by definition.

This means that we are left with friction at the interface between the nanoparticles and the PVA. Due to a weak (chemical) bonding between the gold and the PVA, the nanoparticles might (slightly) slip instead of following all displacements of the PVA. One might even consider a small cavity around the nanoparticles such that they are *shaken* up and down. Both effects would lead to a significant amount of friction at the interface. Considering *shaking* nanoparticles, we are able to explain our observed contrast with a total energy dissipation of 2.79 eV oscillation^{-1} at the nanoparticles, see figure 6.

To get a sense on this experimentally determined value, we compare it with the energy dissipation that occurs in atomic scale friction experiments, in which a sharp tip is laterally moved in contact with a surface [37]. The tip radius in these experiments is comparable to the radius of our nanoparticles! By integrating the stick-slip motion of figure 2(a) in [37], we find a dissipation of approximately 1 eV jump^{-1}, which is associated with the friction when moving the tip only one atomic displacement. For a proper comparison, this value should be multiplied (at least) with a factor of 2, leading to 2 eV jump^{-1}, as we have the complete spheres in contact with the polymer. This value nicely compares with our measured 2.79 eV oscillation^{-1} and definitively reflects the right order of magnitude!

We summarize the effect of friction at the interface between the nanoparticles and the polymer on the amplitude A_{diff} as follows. The dissipated energy per oscillation E_D results in a reduction of the ultrasonic tip amplitude A_s to A_s':

$$A_s' = A_s\sqrt{1 - \frac{2E_D}{kA_s^2}}, \tag{2}$$

in which k is the effective spring constant of the sample. In turn, this leads to a smaller A_{diff}, as $A_{diff} \sim A_t A_s \Big/ \sqrt{A_t^2 + A_s^2}$ [9].

As a remark, we point out that, depending on the roughness of the sample, significant lateral friction can take place between the surface of the sample and the tip. It has even been demonstrated that lateral friction enhances AFM contrasts [38]. However, the friction at the interface between the nanoparticles and the polymer occurs 82 nm *below* the surface. Therefore, lateral friction clearly cannot explain our results, as it is purely a surface effect.

Pinpointing the physical mechanism to friction at *shaking* nanoparticles, we can consider the consequences for the lateral resolution. If one assumes that the propagation in amplitude reduction obeys a scattering-like behavior, the 'fingerprints' of the nanoparticles at the surface should show a significantly larger diameter than the diameter of the nanoparticles. Moreover, as we are measuring in near-field, the size of the 'fingerprints' should be in the order of the depth of the nanoparticles. The deeper the nanoparticle is, the larger should be its image at the surface. These considerations stand in clear contrast to experimental observations: nanoparticles with a diameter of ∼17.5 nm, buried 500 nm deep, are imaged with a diameter of only 20 nm [14], and the imaged fingerprint is even decreasing with increasing depth of the nanoparticles [13]. In contradiction to these observations, the full width half maximum of our observed contrast is approximately equal to the buried depth, exactly as it should be! The reason can be easily understood, if one realizes that we are insensitive to both elasticity variations in the sample and stress fields that can be generated by the tip. The fact that we measure the expected size of the fingerprints confirms one more time that we solely measure the ultrasonic sample vibration in a clean heterodyne detection scheme [9].

Acknowledgments

We gratefully thank Prof R Wördenweber and E Hollmann (Forschungszentrum Jülich, Germany) for the RBS measurements and a first analysis of the data, as well as M Y Yorulmaz for assistance with the sample preparation. The research described in this paper has been performed under and financed by the NIMIC [39] consortium under project 4.4. T H Oosterkamp acknowledges support from an ERC starting grant.

[4] If one would assume a very soft spring between the nanoparticle and the polymer to estimate Raleigh scattering, the resulting contrast is still negligible, as this is similar to a void in the polymer. Therefore, it is the damping parallel to this spring that is mainly responsible for the contrast, which is friction by definition.

Author contributions

The project was initiated and conceptualized by MJR. GJV performed all the measurements, the simulations, and the analytical calculations presented in this study. GJV and MJR interpreted the results and narrowed down the number of possible physical contrast mechanisms. THO helped with the interpretation and suggested 'Friction at shaking nanoparticles' as a possible contrast formation mechanism. GJV and MJR wrote the manuscript together, which was carefully read and improved by all authors.

References

[1] Kolosov O and Yamanaka K 1993 Nonlinear detection of ultrasonic vibrations in an atomic force microscope *Japan J. Appl. Phys.* **32** 1095

[2] Yamanaka K and Nakano S 1996 Ultrasonic atomic force microscope with overtone excitation of cantilever *Japan J. Appl. Phys.* **35** 3787

[3] Cuberes M T, Assender H E, Briggs G A D and Kolosov O V 2000 Heterodyne force microscopy of PMMA/rubber nanocomposites: nanomapping of viscoelastic response at ultrasonic frequencies *J. Appl. Phys.* D **33** 2347

[4] Verbiest G J, van der Zalm D J, Oosterkamp T H and Rost M J 2015 A subsurface add-on for standard atomic force microscopes *Rev. Sci. Instrum.* **86** 033704

[5] Garcia R and Herruzo E T 2012 The emergence of multifrequency force microscopy *Nat. Nanotechnol.* **7** 217–26

[6] Verbiest G J, Oosterkamp T H and Rost M J 2013 Cantilever dynamics in heterodyne force microscopy *Ultramicroscopy* **135** 113–20

[7] Bosse J L, Tovee P D, Huey B D and Kolosov O V 2014 Physical mechanisms of megahertz vibrations and nonlinear detection in ultrasonic force and related microscopies *J. Appl. Phys.* **115** 144304

[8] Ebeling D, Eslami B and Solares S D 2013 Visualizing the subsurface of soft matter: simultaneous topographical imaging, depth modulation, and compositional mapping with triple frequency atomic force microsocpy *ACS Nano* **7** 10387

[9] Verbiest G J and Rost M J 2015 Beating beats mixing in heterodyne detection schemes *Nat. Commun.* **6** 6444

[10] Hu S, Su C and Arnold W 2011 Imaging of subsurface structures using atomic force acoustic microscopy at GHz frequencies *J. Appl. Phys.* **109** 084324

[11] Rabe U *et al* 2002 High-resolution characterization of piezoelectric ceramics by ultrasonic scanning force microscopy techniques *J. Phys. D: Appl. Phys.* **35** 2621

[12] Vitry P *et al* 2015 Mode synthesizing atomic force microscopy for 3D reconstruction of embedded low density dielectric nanostructure *Nano Res.* **8** 072199

[13] Kimura K, Kobayashi K, Matsushige K and Yamada H 2013 Imaging of Au nanoparticles deeply buried in polymer matrix by various atomic force microscopy techniques *Ultramicroscopy* **133** 41

[14] Shekhawat G S and Dravid V P 2005 Nanoscale imaging of buried structures via scanning near-field ultrasound holography *Science* **310** 5745

[15] Cantrell S A, Cantrell J H and Lillehei P T 2007 Nanoscale subsurface imaging via resonant difference-frequency atomic force ultrasonic microscopy *J. Appl. Phys.* **101** 114324

[16] Cuberes M T 2009 Intermittent-contact heterodyne force microscopy *J. Nanomater.* **2009** 762016

[17] Shekhawat G S, Srivastava A, Avasthy S and Dravid V P 2009 Ultrasound holography for noninvasive imaging of buried defects and interfaces for advanced interconnect architectures *Appl. Phys. Lett.* **95** 263101

[18] Tetard L *et al* 2008 Elastic phase response of silica nanoparticles buried in soft matter *Appl. Phys. Lett.* **93** 133113

[19] Tetard L *et al* 2010 Spectroscopy and atomic force microscopy of biomass *Ultramicroscopy* **110** 701

[20] Tetard L, Passian A, Farahi R H and Thundat T 2010 Atomic force microscopy of silica nanoparticles and carbon nanohorns in macrophages and red blood cells *Ultramicroscopy* **110** 586

[21] Tetard L, Passian A and Thundat T 2010 New modes for subsurface atomic force microscopy through nanomechanical coupling *Nat. Nanotechnol.* **5** 105

[22] Tetard L *et al* 2008 Imaging nanoparticles in cells by nanomechanical holography *Nat. Nanotechnol.* **3** 501

[23] Garcia R 2010 Probe microcscopy: images from below the surface *Nat. Nanotechnol.* **5** 101

[24] Verbiest G J, Simon J N, Oosterkamp T H and Rost M J 2012 Subsurface atomic force microscopy: towards a quantitative understanding *Nanotechnology* **23** 145704

[25] Verbiest G J, Oosterkamp T H and Rost M J 2013 Subsurface-AFM: sensitivity to the heterodyne signal *Nanotechnology* **24** 365701

[26] Turner J A, Hirsekorn S, Rabe U and Arnold W 1997 High-frequency response of atomic-force microscope cantilevers *J. Appl. Phys.* **82** 030966

[27] Forchheimer D, Platz D, Tholen E A and Haviland D B 2012 Model-based extraction of material properties in multifrequency atomic force microscopy *Phys. Rev.* B **85** 195449

[28] Platz D, Tholen E A, Pesen D and Haviland D B 2008 Intermodulation atomic force microscopy *Appl. Phys. Lett.* **92** 153106

[29] Platz D, Forchheimer D, Pesen D and Haviland D B 2013 Interaction imaging with amplitude-dependence force spectroscopy *Nat. Commun.* **4** 1360

[30] Rabe U, Janser K and Arnold W 1996 Vibrations of free and surface-coupled AFM cantilevers: theory and experiment *Rev. Sci. Instrum.* **67** 3281

[31] Verbiest G J and Rost M J 2016 Resonance frequencies of AFM cantilevers in contact with a surface *Ultramicroscopy* **171** 70

[32] Parlak Z and Degertekin F L 2008 Contact stiffness of finite size subsurface defects for atomic force microscopy: three-dimensional finite element modeling and experimental verification *J. Appl. Phys.* **103** 114910

[33] Sarioglu A F, Atalar A and Degertekin F L 2004 Modeling the effect of subsurface interface defects on contact stiffness for ultrasonic atomic force microscopy *Appl. Phys. Lett.* **84** 5368

[34] Striegler A *et al* 2011 Detection of buried reference structures by use of atomic force acoustic microscopy *Ultramicroscopy* **111** 1405

[35] Hutter J L and Bechhoefer J 1993 Calibration of atomic-force microscope tips *Rev. Sci. Instrum.* **64** 1868

[36] Santos S *et al* 2011 How localised are energy dissipation processes in nanoscale interactions? *Nanotechnology* **22** 345401

[37] Dienwiebel M *et al* 2004 Superlubricity of graphite *Phys. Rev. Lett.* **92** 126101

[38] Göddenhenrich T, Müller S and Heiden C 1994 A lateral modulation technique for simultaneous friction and topography measurements with the atomic force microscope *Rev. Sci. Instrum.* **65** 2870

[39] http://realnano.nl